JOURNAL OF THERMOPHYSICS AND HEAT TRANSFER
Vol. 24, No. 1, January–March 2010

Technical Notes

Thermal Stress Induced by Inclined Impinging Heating Jet on a Flat Plate

O. Vipat,* X. G. Tian,* T. Kim,* and T. J. Lu*
Xi'an Jiaotong University,
710049 Xi'an, People's Republic of China
and
A. M. Pradeep†
Indian Institute of Technology Bombay,
Powai, Mumbai 400 076, India

DOI: 10.2514/1.45966

Nomenclature

$[C]$	=	elasticity constant matrix
D_h	=	hydraulic diameter of slot, m
F	=	load vector
L	=	flat plate length, m
Re_{Dh}	=	Reynolds number
t	=	flat plate thickness, m
y	=	lateral axis along plate
z	=	axis coinciding with jet center
β	=	relative angle of slot measured from axis parallel to plate, degree
ε	=	strain vector
σ	=	thermal stress, Pa
σ_{yield}	=	yield stress, Pa

I. Introduction

JETS impinging normally on a flat plate have been extensively studied in terms of flow characteristics, wall temperature, and pressure distribution [1,2]. In some cases, a jet impinges on the plate with a certain degree of inclination with respect to the plate, resulting in the oblique impinging jet. In the case of a jet removing heat from the target plate (cooling jet), it has been established that the location of maximum heat transfer shifts increasingly toward the uphill side of the plate, and the maximum Nusselt number decreases as the inclination angle is decreased from the normal impinging position [3,4]. On the contrary, for a heating jet, such an inclination increases the maximum temperature (or heat transfer rate), leading to a significant temperature jump at all the points along the plate [5]. The upward shift of the maximum temperature is attributed to the reduction in effective entrainment of air on both the uphill and downhill sides of the target plate.

Although a multitude of studies have been conducted to characterize the flow and heat transfer characteristics of an impinging jet [1–7], there has not yet been a study devoted to the thermal stresses induced on the target plate by an inclined impinging heating jet. Several systems, including welding, laser heating, and electric discharge machining (EDM), are similar to the impinging heating jet in terms of heat transfer to the target plate and consequently have akin temperature profiles. Yadav et al. [8] used the Galerkin finite element formulation to simulate the EDM-induced temperature and thermal stresses on a target plate. High temperature gradient zones were found to correspond to regions of large stresses that may exceed the material yield strength. Sunar et al. [9] analyzed the temperature and thermal stresses developed in a sheet metal due to welding. The thermal stresses were found to be compressive in nature and follow a trend similar to the temperature distribution due to the high gradients near the center.

The present study is concerned with the thermal stresses developed on a flat plate, due to an impinging heating slot jet, and their variation with jet inclination. For fixed separation distance and Reynolds number, and selected jet inclination angles, the measured temperature data are used as input for thermal stress modeling, using the sequential coupling finite element method (FEM). For a given set of thermal boundary conditions, thermal stresses are calculated for various inclination angles and physical boundary conditions of the plate. The study is limited to the steady-state responses of temperature and thermal stresses.

II. Thermal Stress Modeling

The sequential coupling FEM is adopted to calculate the thermal stresses induced on a flat plate as a result of an impinging heating or cooling jet. Temperature T at an element is approximated in terms of its nodal value T_i^e $(i = 1, 2, \ldots, n)$ as

$$T = N_i^T T_i^e \tag{1}$$

where N_i^T is the shape function and n is the number of element nodes.

For a two-dimensional (2-D) problem, as illustrated in Fig. 1, with the shape function N_i^T serving as the weighted function, the simplified Galerkin weighted residual expression of heat conduction equation is theoretically equal to zero [10]:

$$\int_\Omega N_j^T (k_y T_{,yy} + k_z T_{,zz} + \rho Q)\,\mathrm{d}\Omega - \int_{\Gamma_2} N_j^T (k_y T_{,y} n_y + k_z T_{,z} n_z - q)\,\mathrm{d}\Gamma = 0 \tag{2}$$

Here, k_y and k_z are the thermal conductivity of the plate material along the y and z axes, respectively, n_y and n_z are the unit vectors parallel to the y and z axes, Q is the internal heat generation in the area of Ω, and q is the heat flux imposed through the boundary of Γ_2 (D–A–B–C). It should be noted that the simplified 2-D problem governing Eq. (2) assumes no internal heat generation in the plate, as well as on the adiabatic boundary of Γ_2, except the boundary (C–D) on which the nonuniformly distributed local temperature is prescribed. Substitution of Eq. (1) into Eq. (2) yields:

$$\mathbf{K}\mathbf{T}^e = \mathbf{P} \tag{3}$$

where

$$\mathbf{K} = \sum_e \mathbf{K}^e$$

is the heat conduction matrix, $\mathbf{T}^e = [T_1^e, T_2^e, T_3^e, \ldots, T_{nn}^e]$ is the vector of nodal temperatures,

$$\mathbf{P} = \sum_e \mathbf{P}^e$$

Received 13 June 2009; revision received 3 October 2009; accepted for publication 6 October 2009.

*Ministry of Education Key Laboratory for Strength and Vibration, School of Aerospace.
†Department of Aerospace Engineering.

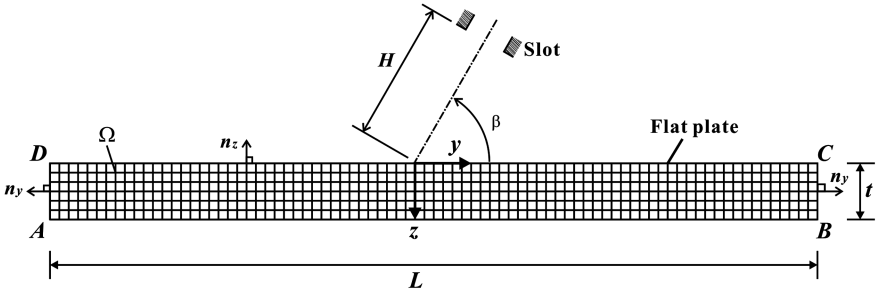

Fig. 1 Computational mesh for calculating thermal stresses on a flat plate.

is the temperature load, and nn is the total number of nodes in the structure of interest. Here, the elements of K^e and P^e are given by

$$K^e_{ij} = \int_{\Omega_e} (k_y N^T_{i,y} N^T_{j,y} + k_y N^T_{i,z} N^T_{j,z})\,\mathrm{d}\Omega,$$
$$P^e_i = \int_{\Omega_e} (N^T_i \rho Q)\,\mathrm{d}\Omega + \int_{\Gamma^e_2} (N^T_i q)\,\mathrm{d}\Gamma \tag{4}$$

Based on the measured temperature on the plate surface ($z = 0$), the temperature distribution in the y–z plane of the plate can be obtained by solving Eq. (3). The constitutive relation for a given plate material can be written as

$$\{\sigma\} = [C][\{\varepsilon\} - \{\beta\}(T - T_0)] \tag{5}$$

where $\{\sigma\}$ is the vector of the thermal stresses, $[C]$ is the matrix of the elastic constants, $\{\varepsilon\}$ is the vector of strains, $\{\beta\}$ is the coefficient of thermal expansion, and T_0 is the reference temperature (ambient temperature).

To solve Eq. (5), the displacement $\{u\}$ in an element needs to be calculated. It is approximated in terms of nodal displacements $\{u^e\}$ and shape function $[N^d]$ as

$$\{u\} = [N^d]\{u^e\} \tag{6}$$

According to the displacement and strain relation, $\varepsilon_{ij} = (u_{i,j} + u_{j,i})/2$, the strain can be expressed as

$$\{\varepsilon\} = [B^d]\{u^e\} \tag{7}$$

where $[B^d]$ is the strain matrix.

The principle of virtual work for steady-state elasticity yields:

$$\int_V \delta\{\varepsilon\}^T\{\sigma\}\,\mathrm{d}V = \int_{A_\sigma} \delta\{u\}^T\{\bar{T}\}\,\mathrm{d}A \tag{8}$$

where $\{\bar{T}\}$ is the traction load on surface A_σ. Substitution of Eqs. (6) and (7) into Eq. (8) leads to

$$\mathbf{K}^d\mathbf{u}^e = \mathbf{F} \tag{9}$$

where

$$\mathbf{K}^d = \sum_e \mathbf{K}^d_e$$

is the stiffness matrix,

$$\mathbf{F} = \sum_e \mathbf{F}^e$$

is the vector of loads, and

$$\mathbf{K}^d_e = \int_V ([N^d]^T[C][N^d])\,\mathrm{d}V \tag{10}$$

$$\mathbf{F}^e = \int_{A_\sigma} ([N^d]^T\{\bar{T}\})\,\mathrm{d}A - \int_V \{[B^d][C]\{\beta\}([N^T]\{T^e\} - T_0)\}\,\mathrm{d}V \tag{11}$$

Note that the load matrix $\mathbf{F}$ contains the thermal loads we have used for temperature analysis. Based on the nodal displacements calculated from Eq. (9), the thermal stresses can be obtained from Eq. (5).

In the present analysis, the thermomechanical problem is treated as plane strain. The plate having in-plane dimensions of 0.13×0.005 m is modeled with eight node plane elements. Before the calculation, the influence of the grid density was checked. Based on the results, in total, 390 elements (78 in y axis and five in z axis) and 1337 nodes are distributed.

For steady-state heat conduction analysis, surface C–D is nonuniformly heated, whereas surfaces A–B, B–C, and D–A are thermally insulated. For thermal stress analysis, four different physical boundary conditions are considered (Table 1). Thermophysical properties of the plate material are listed in Table 2.

III. Discussion of Results

A. Temperature Distributions

Measurements of temperature distribution were performed for a fixed separation distance of $H/D_h = 8$ and selected jet inclination angles of $\beta = 30, 45$, and 90 deg. The jet Reynolds number based on slot hydraulic diameter D_h(=11.3 mm) is fixed at 8.2×10^3. For brevity, only the overall response of the temperature distribution to the variation of jet inclination is described here. Further details,

Table 2 Thermophysical properties of plate material

	Parameter	Value
Thermomechanical properties	Young's modulus	2300 MPa
	Poisson ratio	0.35
	Thermal expansion coefficient	6.75×10^{-5} K^{-1}
	Thermal conductivity	0.21 Wm^{-1} K^{-1}
	Yield stress	62 MPa
Plate dimensions	Length, L	0.13 m
	Thickness t	0.005 m

Table 1 Thermal and physical boundary conditions imposed on a plate

Boundary		A–B	B–C	D–A	C–D
Thermal boundary conditions		Adiabatic	Adiabatic	Adiabatic	Prescribed local temperatures
Physical boundary conditions	case A	Fixed	Traction free	Traction free	Traction free
	case B	Fixed	Traction free	Fixed	Traction free
	case C	Traction free	Fixed	Fixed	Traction free
	case D	Fixed	Fixed	Fixed	Traction free

including flow and pressure characteristics of the impinging jet, can be found in [5].

Figure 2 shows that, at $\beta = 90$ deg, the local temperature peaks at the geometrical stagnation point and its distribution is laterally symmetric relative to this point, with the temperature decreasing monotonically on either side. Furthermore, a decrease in the inclination angle shifts the actual stagnation point toward the uphill side of the plate. The considerable upward shift (or increase) of the wall temperature with the decreasing inclination angle indicates an increase of heat transferred from the hot jet to the plate. Conversely, for an impinging cooling jet, as the inclination angle is decreased from the normal impinging position, heat transfer between the impinging jet and the plate is also decreased [3–7].

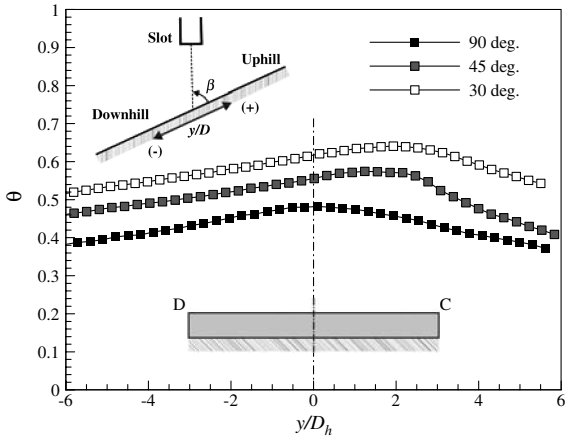

Fig. 2 Lateral distribution of effective temperature along surface C–D under an impinging heating jet with three selected inclination angles, $\beta = 90$ (normal impinging), 45, and 30 deg (Vipat et al. [5]).

B. Thermal Stress Analysis

Jet impingement causes nonuniform temperature distribution as well as nonuniform temperature gradients (Fig. 2). The temperature data are used as input for thermal stress modelling, as discussed in Sec. II. Figure 3a plots the in-plane thermal stress σ on both A–B and C–D surfaces (normalized by the yield stress of plate material σ_{yield}) as a function of the lateral distance away from the geometrical stagnation point (normalized by the jet hydraulic diameter) for $\beta = 30$, 45, and 90 deg and case A (Table 1).

The thermal stress is compressive (as denoted by the negative sign) due to the fact that the heating jet causes significant expansion near the stagnation region that is resisted by the outer regions. At $\beta = 90$ deg, the thermal stress on the C–D surface experiencing the impinging heating jet is laterally symmetric, peaking at the stagnation point. The thermal stress is maximized at the plate center and decreases gradually with increasing lateral distance. Far away from the center, it becomes negligibly small, due to the traction-free boundary conditions. On the other hand, the compressive stress near both ends of the plate, on the physically fixed A–B surface, exhibits a sudden and steep jump with the same distribution and magnitude of the stress observed in the central portion of the plate. It should be noted that, in the present numerical simulation, the plate has a large length-to-thickness ratio ($L/t = 26$). The sudden increase in the compressive stress near both ends of the plate is associated with the fixed physical boundary.

As the inclination angle is decreased, a shift of about 2–3D_h for the peak stress toward the uphill side is observed, consistent with

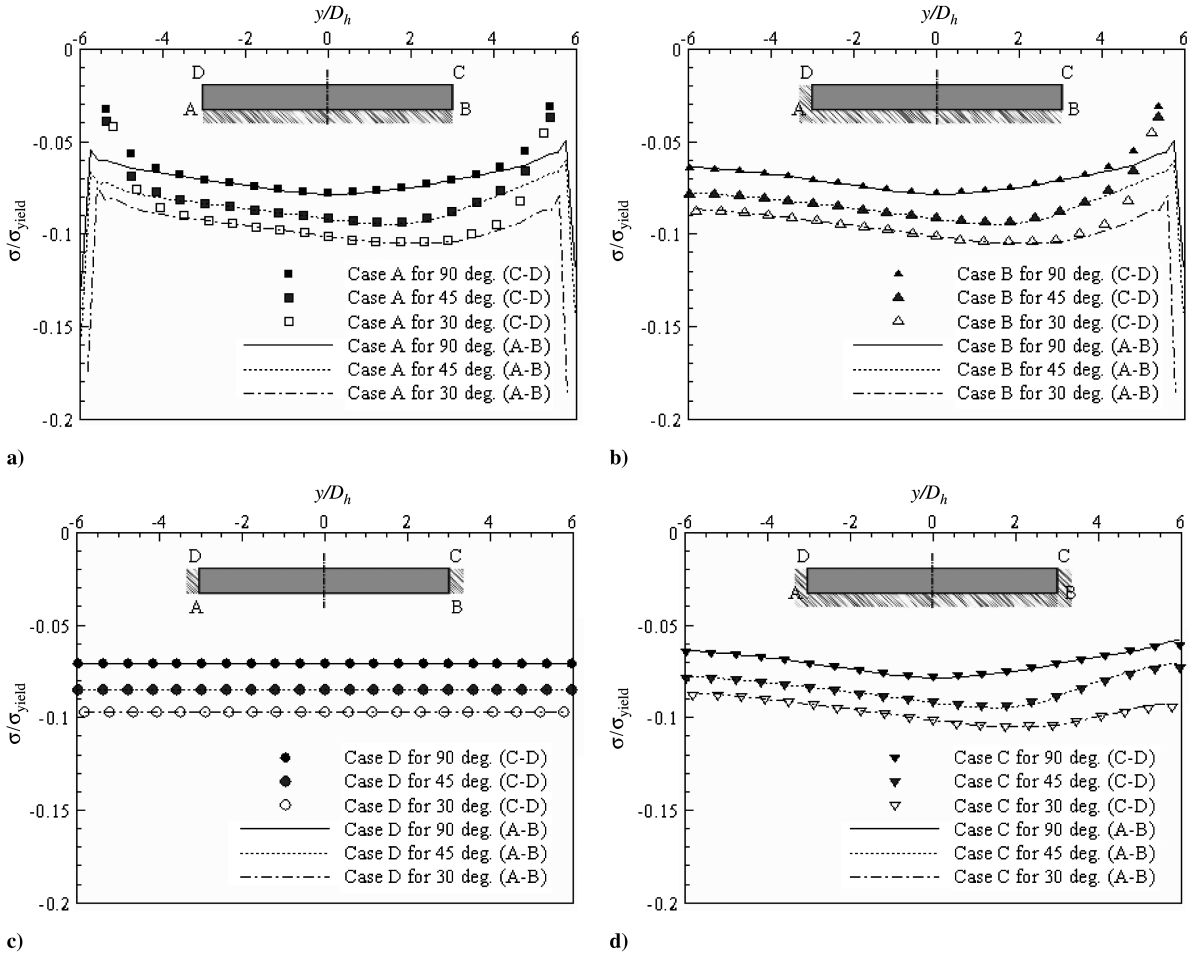

Fig. 3 Lateral distribution of numerically calculated thermal stress on a plate along the A–B and C–D surfaces under different physical boundary conditions: a) case A; b) case B; c) case C; and d) case D.

the shift of the peak temperature. The downward shift of the thermal stress curve with the decreasing β (causing an apparent jump in the thermal stress profile) increases the magnitude of the stress in the near stagnation region. This is due to the high temperature gradient in this region. The thermal stress has large values in the region of $4D_h$ on either side of the plate center, which should be controlled to be smaller than the yield stress of the plate material in practice.

With one of the sidewalls fixed (C–D surface, case B), in addition to case A (Fig. 3b), the traction-free side (B–C) has almost zero stress, whereas the high compressive stresses are induced away from this side due to the fixed boundary condition on the other side (A–D). Near the traction-free edge (i.e., corner B) of the plate on the fixed side, the compressive stress is pronouncedly increased up to approximately twice as high as that generated due to the stagnation of the impinging jet. Jet inclination from the normal impinging position causes an increase of the stress in the entire lateral range.

With the sidewalls (e.g., A–D and B–C) fixed, applicable to both case C and case D, the compressive stress generated on A–B is identical to that on C–D in terms of local distribution and magnitude. With both of the sidewalls fixed (case C) while the A–B surface is traction free, a uniform stress is induced in the entire lateral range of the plate, and the jet inclination leads to a systematic increase of the stress (Fig. 3c). When the A–B surface is fixed, in addition to the physical boundary conditions applied to case C, the compressive stress is maximized within the stagnation region (Fig. 3d). The jet inclination increases the compressive stress with its peak shifted toward the uphill side of the plate, in accordance with the lateral shift of the peak temperature. Under the impinging heating jet, the influence of the jet inclination on the thermal stresses appears to be as significant as the physical boundary conditions applied to each boundary.

We have thus far considered how the nonuniform temperature distribution as a result of the impingement of a heating jet causes the thermal stresses on the target plate in a relatively low temperature range. Particular focus has been placed on the variation of the lateral thermal stress distribution with the inclination of the slot jet. Although it is known that the magnitude of the plate temperature, as well as its gradient, influences the thermal stress field, this is not covered in the present study.

IV. Conclusions

With the temperature profile experimentally obtained serving as input (jet exit-to-plate spacing fixed at $H/D_h = 8$ and Reynolds number at $Re_{Dh} = 8.2 \times 10^3$), the thermal stresses developed on the target plate have been simulated using the sequential coupling FEM. Conclusions drawn from this study are summarized as follows:

1) Compressive stress is induced in the plate under the impinging heating jet. The lateral distribution of the stress is symmetric for the normal impingement ($\beta = 90$ deg).

2) As the inclination angle is decreased, the stress at all lateral points, including the point at which the stress is maximized, is shifted systematically upward.

3) With a given temperature distribution imposed by the impinging heating, the physical boundary conditions of the target plate significantly affect the thermal stresses induced. The contribution of the jet inclination to the stress is comparable with that of the physical boundary conditions.

Acknowledgments

This work is supported by the National Basic Research Program of China (2006CB601203), the National Natural Science Foundation of China (50676075, 10872158), and the National 111 Project of China (B06024).

References

[1] Martin, H., "Heat and Mass Transfer Between Impinging Gas Jets and Solid Surfaces," *Advances in Heat Transfer*, Vol. 13, 1977, pp. 1–60. doi:10.1016/S0065-2717(08)70221-1

[2] Hofmann, H. M., Kind, M., and Martin, H., "Measurements on Steady State Heat Transfer and Flow Structure and New Correlations for Heat and Mass Transfer in Submerged Impinging Jets," *International Journal of Heat and Mass Transfer*, Vol. 50, Nos. 19–20, 2007, pp. 3957–3965. doi:10.1016/j.ijheatmasstransfer.2007.01.023

[3] Beitelmal, A. H., Saad, M. A., and Patel, C. D., "The Effect of Inclination on the Heat Transfer Between a Flat Surface and an Impinging Two-Dimensional Air Jet," *International Journal of Heat and Fluid Flow*, Vol. 21, No. 2, 2000, pp. 156–163. doi:10.1016/S0142-727X(99)00080-6

[4] Eren, H., and Celik, N., "Cooling of a Heated Flat Plate by an Obliquely Impinging Slot Jet," *International Communications in Heat and Mass Transfer*, Vol. 33, No. 3, 2006, pp. 372–380. doi:10.1016/j.icheatmasstransfer.2005.10.009

[5] Vipat, O., Feng, S. S., Kim, T., Pradeep, A. M., and Lu, T. J., "Asymmetric Entrainment Effect on the Local Surface Temperature of a Flat Plate Heated by an Obliquely Impinging 2-Dimensional Jet," *International Journal of Heat and Mass Transfer*, Vol. 52, No. 21–22, 2009, pp. 5250–5257. doi:10.1016/j.ijheatmasstransfer.2009.04.007

[6] Sparrow, E. M., and Lovell, B. J., "Heat Transfer Characteristics of an Oblique Impinging Circular Jet," *Journal of Heat Transfer*, Vol. 102, No. 2, 1980, pp. 202–209. doi:10.1115/1.3244261

[7] Yan, X., and Saniei, N., "Heat Transfer from an Obliquely Impinging Circular Air Jet to a Flat Plate," *International Journal of Heat and Fluid Flow*, Vol. 18, No. 6, 1997, pp. 591–599. doi:10.1016/S0142-727X(97)00051-9

[8] Yadav, V., Jain, V. K., and Dixit, P. M., "Thermal Stresses due to Electrical Discharge Machining," *International Journal of Machine Tools and Manufacture*, Vol. 42, No. 8, 2002, pp. 877–888. doi:10.1016/S0890-6955(02)00029-9

[9] Sunar, M., Yilbas, B. S., and Boran, K., "Thermal and Stress Analysis of a Sheet Metal in Welding," *Journal of Materials Processing Technology*, Vol. 172, No. 1, 2006, pp. 123–129. doi:10.1016/j.jmatprotec.2005.09.008

[10] Wang, X., and Shao, M., *The Basic Principle of Finite Element Method and Numerical Method*, Tsinghua Univ. Press, Beijing, 1997.